Journal of CO2 Utilization 57 (2022) 101881

Contents lists available at ScienceDirect

Journal of CO2 Utilization

journal homepage: www.elsevier.com/locate/jcou

Restructuring Ni/Al_2O_3 by addition of Ga to shift product selectivity in CO_2 hydrogenation: The role of hydroxyl groups

Ali M. Bahmanpour [a], Rob Jeremiah G. Nuguid [a,b], Louisa M. Savereide [a], Mounir D. Mensi [a], Davide Ferri [b], Jeremy S. Luterbacher [a], Oliver Kröcher [a,b,*]

[a] Institute of Chemical Sciences and Engineering, École Polytechnique Fédérale de Lausanne (EPFL), 1015 Lausanne, Switzerland
[b] Paul Scherrer Institute, 5232 Villigen, PSI, Switzerland

ARTICLE INFO

Keywords:
CO_2 hydrogenation
Nickel
Gallium
Reverse water gas shift reaction
Methanation
Hydroxyl group

ABSTRACT

Ni/Al_2O_3 is an active catalysts for CO_2 hydrogenation to both CH_4 and CO. By doping with Ga, we succeeded in shifting the selectivity of these catalysts almost completely toward CO. *In-situ* IR spectroscopy studies showed that the catalyst activity is directly related to the concentration of surface hydroxyl groups that are responsible for the adsorption of CO_2 and the formation of intermediate bicarbonates and formates on the catalyst surface. The addition of Ga improved the Ni dispersion which was concomitant with the formation of a Ni-Ga layer on the surface of alumina, thereby reducing the surface hydroxyl concentration. The reduced and weakened interaction between the intermediate products, i.e. bicarbonates and formates, and the catalyst surface, increased the CO selectivity from ~40 % to 98 %.

1. Introduction

CO_2 capture and utilization is an important option for a future carbon-neutral economy as excessive CO_2 emissions affect the climate and the environment [1,2]. The catalytic conversion of CO_2 to value-added chemicals is one of the most promising and researched approaches. In combination with renewable hydrogen, the conversion of CO_2 into fuels can help close the carbon cycle. Various products such as alcohols, acids, aldehydes, and olefins have been synthesized through thermal, electrical and photochemical CO_2 conversion [3–8]. Among such products, CO_2 hydrogenation to CO, also known as the reverse water-gas shift reaction (RWGS, Eq. 1), has attracted attention since CO is more active than CO_2 and can be further hydrogenated to variety of products [9–13].

$$CO_2 + H_2 \leftrightarrow CO + H_2O \quad \Delta H = 41.2\ kJ.mol^{-1} \tag{1}$$

After conversion to CO, CO_2 can be converted into light olefins as well as jet fuel through further hydrogenation in the Fischer-Tropsch reaction [14]. In addition, the RWGS is part of a pathway to form methanol as a CO_2 hydrogenation product [15–19]. Many catalysts have been used for CO_2 conversion to CO. In general, transition metals of the groups 8–10 such as Ni, Pd, Ru, and Rh have been shown to form both CO and CH_4, while group 11 metals such as Cu, Ag and Au produce CO more selectively [20]. In particular, Cu-based and Mo-based catalysts were found to catalyze the almost exclusive formation of CO [9,21–25]. Metal-carbides, nitrides, and phosphides can also form active structures for CO_2 hydrogenation reactions [26–28]. Among various catalysts, certain patterns have been observed. For instance, although nanoparticles of group 8–10 transition metals form both CO and CH_4, atomic dispersion of the metals shifts their selectivity towards CO formation [29–31]. However, the oxidation state of the metal sites can also affect the product selectivity [32]. The addition of promoters to improve the catalyst activity and stability was also studied in detail [33–42]. Reina's group investigated the addition of Cu and Cs promoters to Mo_2C to increase the catalyst activity for the RWGS reaction [12,13]. The addition of Cu added more active sites, whereas the addition of electropositive Cs shifted the electron density favorably. The addition of alkali metals as electropositive elements has the same positive shifting effect on the electron density in the case of the RWGS reaction [43]. Other transition metals were used to form bimetallic catalysts, which promote the CO selectivity and/or catalyst activity for CO_2 hydrogenation [33,44]. Ni-based catalysts have been studied extensively for hydrogenation reactions, since they are relatively inexpensive and active materials. They tend to form both CO and CH_4, but are mostly used for catalyzing the CO_2 conversion to CH_4 (Sabatier reaction). If Ni-based catalysts could be tuned to selectively produce CO, they would be a favorable RWGS

* Corresponding author at: Institute of Chemical Sciences and Engineering, École Polytechnique Fédérale de Lausanne (EPFL), 1015 Lausanne, Switzerland.
E-mail address: oliver.kroecher@psi.ch (O. Kröcher).

https://doi.org/10.1016/j.jcou.2021.101881
Received 25 November 2021; Received in revised form 22 December 2021; Accepted 29 December 2021
Available online 7 January 2022

catalysts since they are more robust at higher temperatures compared to Cu-based catalysts [45]. This is an important property since the endothermic RWGS reaction requires high temperatures, at which Cu-based catalysts suffer from low stability [9]. There have been successful attempts to shift the selectivity of CO_2 hydrogenation toward CO on modified Ni-based catalysts. Le Saché et al. synthesized a Ru-Ni/-CeO_2-ZrO_2 catalyst with which they achieved 91 % CO selectivity, but only at high temperatures (750 °C) [46]. Braga et al. also promoted Ni by addition of Pd. They managed to reach up to 45 % CO selectivity at 600 °C [47].

In this context, Cammarota et al. noticed that the addition of Ga to Ni can stabilize formate on Ni during the CO_2 hydrogenation reaction [48]. Formate has been reported to be one of the intermediates in the RWGS. Although this study was carried out with homogeneous catalysts and under high pressures (34 atm), it motivated us to consider the addition of Ga to Ni to form a Ni-based catalyst with potentially high selectivity towards CO. Following this concept, we prepared a Ni-Ga catalyst on an alumina support that produces CO almost completely selectively (98 % selectivity) at a relatively low temperature (400 °C). We also studied the reaction mechanism on both Ni/Al_2O_3 and $Ni\text{-}Ga/Al_2O_3$ using in-situ diffuse reflectance infrared Fourier transform spectroscopy (DRIFTS), from which we concluded that the presence of hydroxyl groups on the surface strongly influences the activity of the catalyst in CO_2 conversion.

2. Experimental

2.1. Catalysts synthesis

The supported Ni-Ga catalysts as well as the control catalyst (Ni/Al_2O_3) were synthesized by means of the incipient wetness impregnation method based on a previously published study [49]. The desired amounts of $Ni(NO_3)_2{\bullet}6H_2O$ (Sigma-Aldrich) and $Ga(NO_3)_3{\bullet}9H_2O$ (Sigma-Aldrich) were used as metal precursors and γ-alumina (Merck) was used as the support. For instance, 2.48 g of nickel precursor and 3 g of gallium precursor was used for the preparation of $1Ni\text{-}1Ga/Al_2O_3$. The amount of Ni was constant for all catalysts while the amount of Ga was varied. The procedure for the synthesis of Ga/Al_2O_3 was the same as for the other catalysts except that no Ni was added to this catalyst. The actual loadings are presented in Table S1 in the Supporting information. The catalysts were dried at 120 °C overnight and calcined at 700 °C for 6 h with a temperature ramp of 5 °C min^{-1}.

2.2. Catalytic activity tests

The catalytic activity tests were performed using a laboratory test bench with a fixed-bed quartz tube reactor with heating wires and a temperature controller. The outlet stream was analyzed with an online MATRIX-MG01 FTIR spectrometer (Bruker) with a 10 cm gas cell, heated at 120 °C. The spectrometer was operated with the OPUS-GA software to evaluate the spectra. For each test, 100 mg of catalyst was fixed in the reactor using quartz wool. The catalyst was reduced at the desired temperature (heating ramp 10 °C min^{-1}) *in-situ* for 1 h under 20 % H_2 flow diluted in Ar prior to each test. After reduction, the temperature was set to 400 °C and a mixture of CO_2 and H_2 diluted in Ar was dosed into the reactor. The CO_2:H_2 ratio was set to 1:4 with a weight hourly space velocity (WHSV) of 30,000 mL•g_{cat}^{-1} h^{-1}.

For the OH passivation test on Ni/Al_2O_3, the same procedure as above was used. However, after reduction at 700 °C, the catalyst was exposed to 10 mL min^{-1} of CO diluted in Ar. The temperature was set to 350 °C to avoid the formation of nickel tetracarbonyl ($Ni(CO)_4$), which forms at temperatures lower than 230 °C [50]. During CO introduction, the formation of CO_2 was monitored and when no more CO_2 was detected in the in-line FTIR, the reactor was purged with Ar for 30 min. The temperature was then set to 700 °C with a 10 °C min^{-1} ramp to desorb potentially adsorbed CO from the surface of the catalyst. The temperature was set again to 400 °C and the same reaction mixture of CO_2 and H_2 was used at the above mentioned conditions. At the end of the test, the Ni content of the sample was checked with ICP-OES to ensure no Ni was lost in form of $Ni(CO)_4$ during the passivation process (Table S1).

2.3. Catalyst characterization

Barrett-Joyner-Halenda (BJH) mesoporous volumes and Brunauer-Emmett-Teller (BET) surface areas were calculated from N_2 physisorption isotherms collected with a Micromeritics 3Flex instrument. Before measurements, all materials were degassed overnight under vacuum ($<10^{-3}$ mbar) at 120 °C (10 °C min^{-1} ramp rate).

Hydrogen Temperature Programmed Reduction (H_2-TPR) profiles was recorded on a Micromeritics Autochem 2920 II instrument. Typically, the samples (~400 mg) were diluted with silicon carbide (~250 mg), loaded into a quartz U-shaped quartz cell, and dried under He (50 mL min^{-1}) at 150 °C. After cooling to 40 °C under He, the samples were heated to 900 °C at a ramp of 10 °C min^{-1} under a flow of 10 % H_2 with balance Ar (50 mL min^{-1}). The effluent gasses were passed through a cold trap with a mixture of liquid N_2 and ethanol, and H_2 consumption was monitored with a TCD.

Additional H_2-TPR experiments were carried out using a slightly modified procedure. Fresh samples (~100 mg diluted in 500 mg silicon carbide) were dried and cooled under He as before. Then, the samples were heated to 700 °C (10 °C min^{-1}) and held at temperature for 1 h under a flow of dilute H_2 (10 % H_2, bal. Ar, 50 mL min^{-1}). The samples were cooled under He, and reheated again at 10 °C min^{-1} to 900 °C under dilute H_2.

Diffuse reflectance infrared Fourier transform (DRIFT) spectra were collected using a Bruker Vertex70 spectrometer equipped with a liquid nitrogen-cooled HgCdTe detector. The spectra were recorded from 4000 to 1000 cm^{-1} at a resolution of 4 cm^{-1} and scanner velocity of 80 kHz. The sample and background spectra resulted from averaging 10 and 100 scans, respectively. Approximately 30−40 mg of the catalyst sample were placed in a custom-built spectroscopic cell with a low void volume [51]. The cell was equipped with a 2-mm-thick CaF_2 window (Crystran) and attached to a Praying Mantis™ accessory (Harrick Scientific) in the compartment of the IR spectrometer. Prior to the *in-situ* experiments, the sample was activated under 80 vol% H_2/Ar flow for 30 min. The subsequent steps were as follows: (1) introduction of 7 vol% CO_2 at 250 °C; (2) removal of 7 vol% CO_2 at 250 °C with Ar; (3) ramp-up to 350 °C under Ar; (4) introduction of 7 vol% CO_2 and 30 vol% H_2 at 350 °C; (5) removal of 7 vol% CO_2 and 30 vol% H_2 at 350 °C.

The X-ray photoelectron spectroscopy (XPS) measurements were carried out on an Axis Supra (Kratos Analytical) using the monochromated Kα X-ray line of an aluminum anode. The pass energy was set to 40 eV with a step size of 0.15 eV. The samples were electrically insulated from the sample holder and charges were compensated. Spectra were referenced at 284.8 eV using the C 1s orbital of the C—C bond. Before XPS measurements, the samples were reduced for 1 h at 700 °C with the same flowrates as indicated in the catalytic experiments. The samples delivered to the instrument were prepared using a glovebox to ensure no air exposure occurred.

Data for X-ray diffraction (XRD) were acquired using a D8 Bruker Discover diffractometer, which was equipped with a LynxEye XE detector as well as a non-monochromated Cu-source. The XRD patterns were measured for 2θ between 10 ° and 80 ° with the step size of 0.01.

High-Angle Annular Dark-Field Scanning Transmission Electron Microscopy (HAADF-STEM) was conducted on a FEI Talos with 200 kV acceleration voltage in the Z contrast mode. Samples were dispersed in ethanol and placed on a carbon coated copper grid. Energy-Dispersive X-ray Spectroscopy (EDXS) analysis was performed using Bruker Esprit software.

3. Results and discussion

3.1. Catalytic activity

While Ni nanoparticles tend to dissociate C and O on their surface, addition of Ga to Ni has been shown to suppress this effect [49]. In order to study the effect of Ga addition to Ni on its catalytic activity and product selectivity, we synthesized three alumina-supported catalysts with various Ni to Ga molar ratios, i.e. 1Ni–1Ga/Al_2O_3 (Ni:Ga = 1:1), 2Ni–1Ga/Al_2O_3 (Ni:Ga = 2:1), and 1Ni–2Ga/Al_2O_3 (Ni:Ga = 1:2), and tested them for CO_2 hydrogenation. The measured CO_2 conversions and the selectivities to CO and CH_4 are presented in Fig. S1 in the Supporting information. The CO selectivity of these catalysts followed the order: 1Ni–2Ga/Al_2O_3 ≅ 1Ni–1Ga/Al_2O_3 > 2Ni–1Ga/Al_2O_3 (selectivities are reported in Table S2) and the CO_2 conversion was almost the same for all three, but was slightly higher for 1Ni–2Ga/Al_2O_3 (9 %) and 2Ni–1Ga/Al_2O_3 (9.5 %) compared to 1Ni–1Ga/Al_2O_3 (7 %). This means that the overall best performing candidate in terms of both activity and selectivity was 1Ni–2Ga/Al_2O_3, which was selected for further studies. The CO_2 conversion rate of these studied catalysts are presented in Table S2 for comparison. The structure of these catalysts as well as the reference Ni/Al_2O_3 catalysts were studied by X-ray Diffraction (XRD) and the patterns are presented in Fig. S2. No clear peaks of Ni or NiO were detected, which supports the high dispersion of Ni on all catalysts. Fig. 1 shows the CO_2 conversion and CO selectivity for 1Ni–2Ga/Al_2O_3 and Ni/Al_2O_3 as the reference catalyst. Ga/Al_2O_3 was also tested as a reference but only insignificant CO_2 conversion (<2 %) was detected on this catalyst. The low conversion of CO_2 on Ga/Al_2O_3 is caused by the lack of active nickel sites for H_2 adsorption and dissociation. While the CO_2 conversion was clearly higher using Ni/Al_2O_3 compared to 1Ni–2Ga/Al_2O_3 (~30 % as opposed to 10 %), its CO selectivity was significantly lower compared to 1Ni–2Ga/Al_2O_3 (~40 % as opposed to 98 %). The addition of Ga caused the shift of selectivity to CO, resulting in the observed decreased conversion level since the methanation reaction almost ceased. To compare the CO selectivity using various catalysts, they should be tested in the same range of CO_2 conversion. Therefore, we have decreased the WHSV for 1Ni-2Ga/Al_2O_3 (Fig. S3), to bring its level of CO_2 conversion close to the one reported for Ni/Al_2O_3 in Fig. 1. We observed that the CO selectivity on this catalyst did not change compared to Fig. S1 despite its higher CO_2 conversion.

3.2. In-situ DRIFTS results

When using alumina-supported transition metals as catalysts, the RWGS reaction mechanism is known to proceed through CO_2 adsorption (forming carbonate or bicarbonate) followed by its reaction with dissociated H atoms to form oxygenated intermediate products (formate or carboxylate). The formed intermediate product then decomposes to form CO and H_2O [52–55]. In order to understand the reasons behind the differences in the performance of the presented catalysts, we studied the reaction mechanisms by means of *in-situ* DRIFTS experiments. The IR spectra were collected when introducing and purging CO_2 as well as during the CO_2 hydrogenation reaction and reactant cut-off.

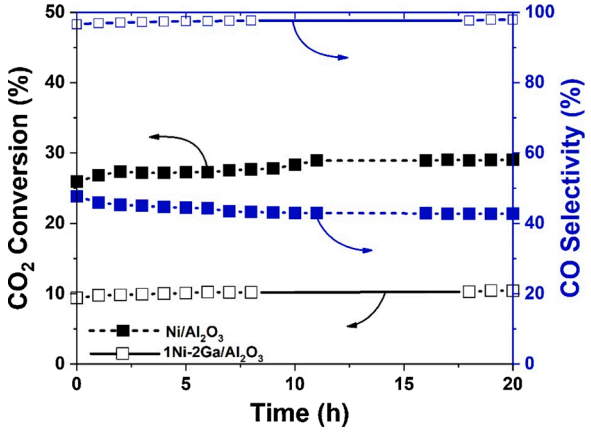

Fig. 1. CO_2 conversion and CO selectivity for Ni/Al_2O_3 and 1Ni-2Ga/Al_2O_3. Reduction T = 700 °C. Reaction T = 400 °C.

Fig. 2a and b shows the IR spectra obtained during the adsorption of CO_2 on 1Ni-2Ga/Al_2O_3 and Ni/Al_2O_3. The persistence of the peaks at 2344 and 2358 cm^{-1} reflects the continuous presence of gas-phase CO_2. For both samples, we observed two peaks at 1649 cm^{-1} and 1442 cm^{-1}, which together with the weak signal at 1220 cm^{-1}, are characteristic for the formation of bicarbonates [54] formed through the reaction of CO_2 with surface hydroxyl groups. However, the area of the bicarbonate peak at 1649 cm^{-1} over Ni/Al_2O_3 was up to 23 % larger than that over 1Ni-2Ga/Al_2O_3, suggesting that Ga incorporation results in less CO_2 uptake and adsorption (Fig. S4). Since bicarbonates are formed due to the interaction of CO_2 with surface hydroxyl groups, this observation points out that there are fewer hydroxyl species in the Ga-containing sample. Indeed, the single-beam spectrum of 1Ni-2Ga/Al_2O_3 showed comparatively less hydroxyl groups than on Ni/Al_2O_3 (Fig. S5). Therefore, it is reasonable to conclude that the surface hydroxyl groups control the adsorption CO_2 and the formation of bicarbonate as the intermediate product. This observation explains the lower activity of 1Ni-2Ga/Al_2O_3 for CO_2 hydrogenation.

Fig. 2c and d shows the spectra obtained during desorption of CO_2 from 1Ni-2Ga/Al_2O_3 and Ni/Al_2O_3. The abrupt disappearance of the gas-phase CO_2 peaks was accompanied by a much slower extinction of the peaks at 1649 cm^{-1} and 1442 cm^{-1}, which suggests the desorption of bicarbonate species. The bicarbonates almost fully desorbed from 1Ni-2Ga/Al_2O_3 after 10 min of purging while a significant portion remained bound to Ni/Al_2O_3. According to literature, stronger adsorption of the intermediate products results in their further hydrogenation to CH_4 [56]. This explains the increased CH_4 formation on Ni/Al_2O_3, where residual bicarbonate species persisted after CO_2 removal. In contrast, only weakly adsorbed CO_2 participates in the formation of CO through the RWGS [24]. Hence, the weaker interaction of 1Ni-2Ga/Al_2O_3 with the bicarbonate species proved to be beneficial in driving the selectivity towards CO.

The weak adsorption of CO_2 on 1Ni-2Ga/Al_2O_3 can be explained by the structure of this catalyst. Fig. 3 shows the STEM images of the 1Ni-2Ga/Al_2O_3 catalyst. While both small and relatively large Ni nanoparticles were formed on Ni/Al_2O_3 (Fig. 4), a uniform dispersion of Ni and Ga was observed on 1Ni-2Ga/Al_2O_3. The STEM images in Fig. 3 suggest that Ni and Ga have mostly covered the surface of alumina since the blue color representing Al is not prominent on the edge of the STEM images on Fig. 3. Highly dispersed transition metals can only weakly adsorb the intermediate products of CO_2 hydrogenation and therefore, selectively form CO [31].

The aforementioned alumina surface coverage is also supported by N_2 physisorption results (Figs. S6 and S7 as well as Table 1). Through comparison of the BET surface area (S_{BET}) and pore volume (V_p), we noted that impregnation of Ni on alumina did not change the initial surface area (120 m^2 $g^{-1}$for Al_2O_3 and 117 m^2 g^{-1} for Ni/Al_2O_3) and pore volume (0.232 cm^3 g^{-1} for Al_2O_3 and 0.226 cm^3 g^{-1} for Ni/Al_2O_3) of alumina. However, for 1Ni-2Ga/Al_2O_3, both S_{BET} and V_p decreased to 102 m^2 g^{-1} and 0.1798 cm^3 g^{-1}, respectively. Although this decrease in surface area as well as pore volume is not very pronounced, it may be due to the formation of a Ni-Ga entities on the catalyst surface, which blocked some of the pores and consequently decreased the surface area. Therefore, we hypothesize that the formation of the Ni-Ga layer may have decreased the availability of the Al_2O_3 surface and caused the aforementioned decrease in hydroxyl group concentration. This hypothesis was also checked using Al 2p XPS spectra (Fig. S8). It can be noted that the signal intensity for Al 2p decreased for 1Ni-2Ga/Al_2O_3 compared to Ni/Al_2O_3, which supports the formation of the Ni-Ga layer.

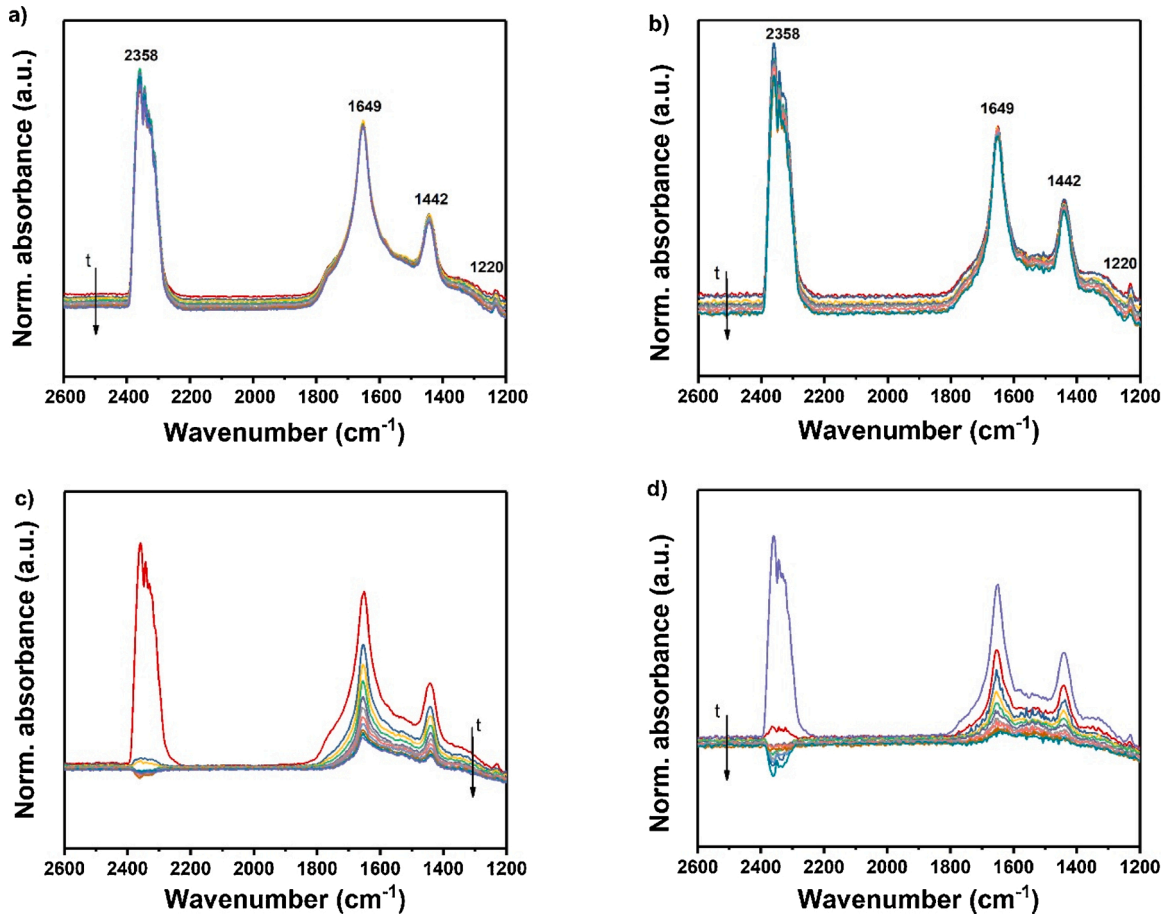

Fig. 2. Time series of IR spectra after the dosage of CO_2 on a) Ni/Al_2O_3 and b) $1Ni\text{-}2Ga/Al_2O_3$. Time series of IR spectra during desorption of CO_2 from c) Ni/Al_2O_3 and d) $1Ni\text{-}2Ga/Al_2O_3$. T = 250 °C. Total acquisition time for each spectral series was 10 min with 1 min intervals between the individual spectra.

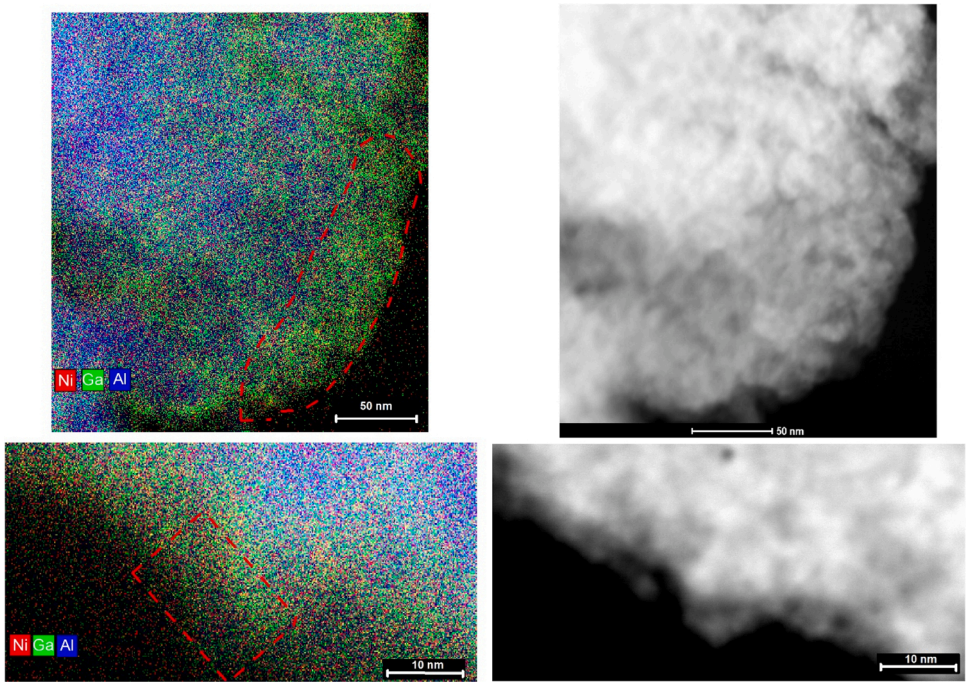

Fig. 3. STEM images of $1Ni\text{-}2Ga/Al_2O_3$.

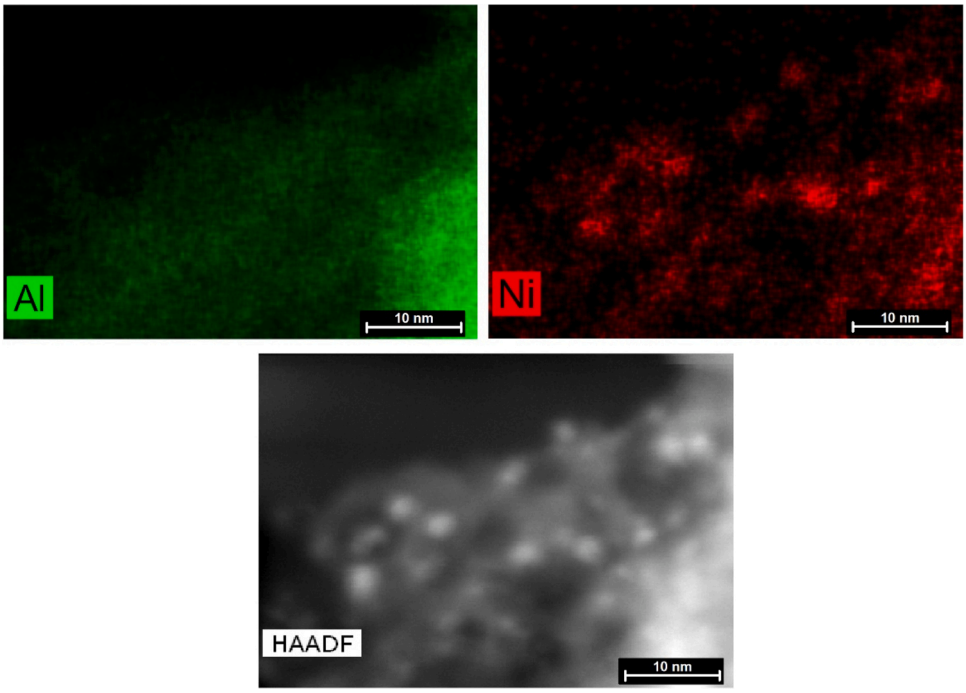

Fig. 4. STEM images of Ni/Al_2O_3.

Table 1
N_2 physisorption data for Ni/Al_2O_3, $1Ni\text{-}2Ga/Al_2O_3$, and Al_2O_3.

Catalysts	S_{BET} ($m^2 \cdot g^{-1}$)	V_p ($cm^3 \cdot g^{-1}$)
Ni/Al_2O_3	117	0.226
$1Ni\text{-}2Ga/Al_2O_3$	102	0.179
Al_2O_3	120	0.232

The CO_2 hydrogenation reaction was studied with IR spectroscopy and the results are shown below (Fig. 5). After introduction of H_2 on both catalysts, the peaks at 1649 cm^{-1} and 1442 cm^{-1} started to disappear and peaks at 1595 cm^{-1}, 1393 cm^{-1} and 1375 cm^{-1} formed, which indicate the presence of formate species [57]. We concluded that bicarbonate was hydrogenated to formate upon H_2 introduction, in line with previously reported CO_2 hydrogenation studies on Au/Al_2O_3 [52]. A higher formate concentration was detected on $1Ni\text{-}2Ga/Al_2O_3$ compared to Ni/Al_2O_3, as evidenced by the higher ratio of the peak areas for formate (1595 cm^{-1}) and bicarbonate (1649 cm^{-1}). This means that nickel alone is more capable of activating adsorbed formate species than Ni-Ga, resulting in the observed higher concentration of surface formate on the Ga-treated catalyst. This explanation is also confirmed by the spectral response upon gas cut-off (Fig. 5c and d). When the gas flows were cut off, unreacted formate on both catalyst surfaces were observed, which suggests that at least some formate species remains on the catalyst surface as spectator species, most probably those formate species far distant from Ni. Formate is also known to be a potential intermediate for the methanation reaction [56]. Therefore, we propose that the formates that remain unreacted on the $1Ni\text{-}2Ga/Al_2O_3$ surface, poisoned some of the active sites, which resulted in the lower activity of this catalyst. The same species react further to form methane on the Ni/Al_2O_3 catalyst, which lowers the relative selectivity of this catalyst compared to those containing Ga.

3.3. Investigation of the effect of the hydroxyl groups

Based on the results obtained from the in-situ investigation of the catalysts, the concentration of hydroxyl groups were found to be correlated with the adsorption of CO_2. To further test the importance of these surface groups for CO_2 hydrogenation, we passivated the hydroxyl groups on the surface of Ni/Al_2O_3 using an approach described by Yang et al. [58]. Their method consists of reacting the OH groups with CO to remove them from the catalyst surface through the water-gas shift reaction (WGS) (details are described in Section 2.2). Fig. 6 shows the activity of Ni/Al_2O_3 for CO_2 hydrogenation with and without passivation with CO. Importantly, the CO_2 conversion on the CO-passivated catalyst decreased compared to the non-passivated catalyst. This further confirms the effect of the hydroxyl groups on adsorption of CO_2. Both the IR spectroscopy results and the CO passivation results indicate that the presence of hydroxyl groups facilitates the CO_2 adsorption through formation of bicarbonate, which in turn results in higher CO_2 conversion. Al_2O_3 not only provides a large surface area for the dispersion of metallic active sites for the adsorption and dissociation of H_2, but also supports the presence of hydroxyl groups on the catalyst surface that can actively react with CO_2 and thus participate in the reaction.

3.4. Investigation of catalysts structure

To better understand the relationship of structure and activity, the surfaces of $1Ni\text{-}2Ga/Al_2O_3$ and Ni/Al_2O_3 were investigated by XPS. Since the catalysts were reduced *in-situ* before the catalytic tests, we reduced the catalysts under the same conditions before the XPS measurements. The Ni 2p spectra for both catalysts are presented in Fig. 7. The presence of Ga on the surface of $1Ni\text{-}2Ga/Al_2O_3$ is evident from the Ga 2p spectra (Fig. S9). Ni on the surface of $1Ni\text{-}2Ga/Al_2O_3$ appears to be mostly reduced and present in metallic form. However, the Ni 2p spectrum for Ni/Al_2O_3, shows that Ni was not fully reduced on this catalyst, where it was predominantly present as NiOOH and $Ni(OH)_2$. Ni 2p fitting was performed based on the approach of Biesinger et al. [59]. While CO_2 adsorption on Ni/Al_2O_3 could be facilitated due to the presence of the hydroxyl groups, H_2 adsorption and activation is less favorable in the absence of metallic Ni. Considering the similar Ni loading and the same reduction conditions, this observation demonstrates that Ga promotes the reducibility of Ni.

The reducibility of these catalysts were further studied in H_2-TPR experiments. In our first experiment, the calcined catalysts were reduced

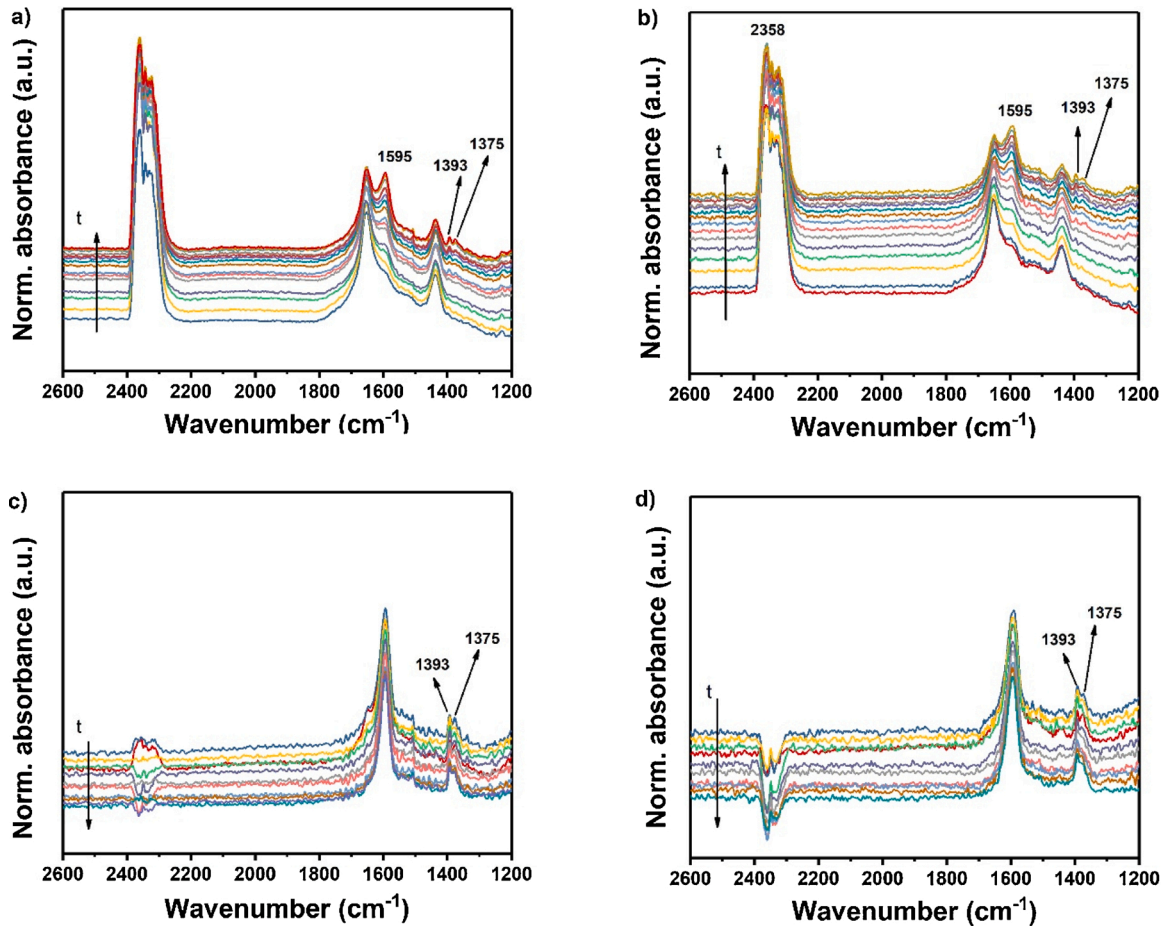

Fig. 5. Time series of IR spectra after CO_2 and H_2 reaction on a) Ni/Al_2O_3 and b) $1Ni\text{-}2Ga/Al_2O_3$. Time series of IR spectra after gas flow cut-off on c) Ni/Al_2O_3 and d) $1Ni\text{-}2Ga/Al_2O_3$. T = 350 °C. Total acquisition time for each spectral series was 15 min with 1 min intervals between the individual spectra.

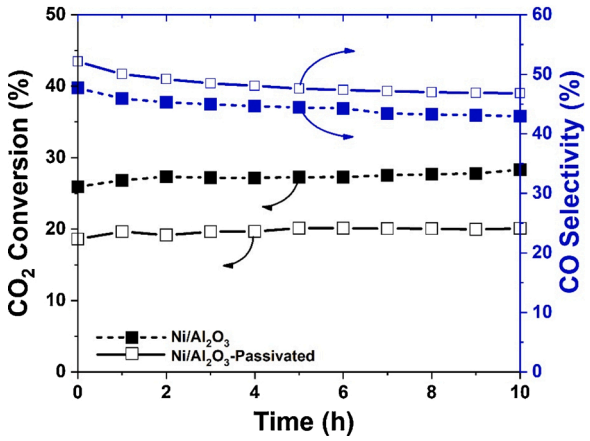

Fig. 6. CO_2 conversion and CO selectivity for Ni/Al_2O_3 and passivated Ni/Al_2O_3 using CO. Reduction T = 700 °C. Reaction T = 400 °C.

up to 900 °C. It is clearly visible from Fig. 8 that the reduction of $1Ni\text{-}2Ga/Al_2O_3$ starts at lower temperatures compared to Ni/Al_2O_3 (~520 °C as opposed to ~600 °C). This confirms the promoting role of Ga for the reducibility of Ni. In the second experiment, we conducted H_2-TPR on both catalysts after reducing them under the same conditions used during the catalytic tests (20 vol% H_2/He flow at 700 °C for 1 h). The results showed that both catalysts were partly reduced during this treatment (Fig. S10). However, by comparison with the H_2-TPR profiles for the calcined catalysts, we observed that most of the Ni on $1Ni\text{-}2Ga/Al_2O_3$ was already reduced during the pre-treatment, while a notable portion of the Ni sites of Ni/Al_2O_3 catalyst remained unreduced after the pre-treatment. This is also in agreement with the aforementioned XPS results (Fig. 7).

As observed in the H_2-TPR profiles, the peak of H_2 consumption for both catalysts occurred at 830 °C, which ensured the full reduction of Ni sites. Since, based on XPS results, the Ni sites on the surface of $1Ni\text{-}2Ga/Al_2O_3$ were mostly reduced, we did not expect much variation in catalyst activity after reduction at 830 °C. For Ni/Al_2O_3, however, a higher catalyst activity would be expected compared to the treatment at 700 °C, since metallic Ni has higher H_2 adsorption and dissociation activity. To study these effects, we performed the same catalytic test but with *in-situ* catalyst reduction at 830 °C for 1 h prior to the test (Fig. 9). The Ni/Al_2O_3 catalyst activity increased after this treatment (initial CO_2 conversion was 33 % as opposed to 26 % in Fig. 1). As expected, for $1Ni\text{-}2Ga/Al_2O_3$ catalyst, little change was observed. Our results and corresponding discussions in the literature confirm that two groups of active sites are required for the RWGS reaction. One serves for adsorption and dissociation of H_2 molecules, the other for adsorption of CO_2. The metal sites (e.g., on Ni/Al_2O_3 and $1Ni\text{-}2Ga/Al_2O_3$) are responsible for the adsorption and dissociation of H_2. A lack of these sites is the reason for the low activity of Al_2O_3 or Ga_2O_3/Al_2O_3. However, for high selectivity of Ni-based catalysts in CO formation, high dispersion of the metallic sites is required. Otherwise, accumulation of the metallic Ni sites may lead to the formation of CH_4. On the other hand, the presence of hydroxyl groups on the metal oxide (Al_2O_3 in this case) is required to adsorb CO_2, as shown by the DRIFTS study.

We did not observe any deactivation in any of the catalytic tests we performed. However, we investigated the spent catalysts with XRD for

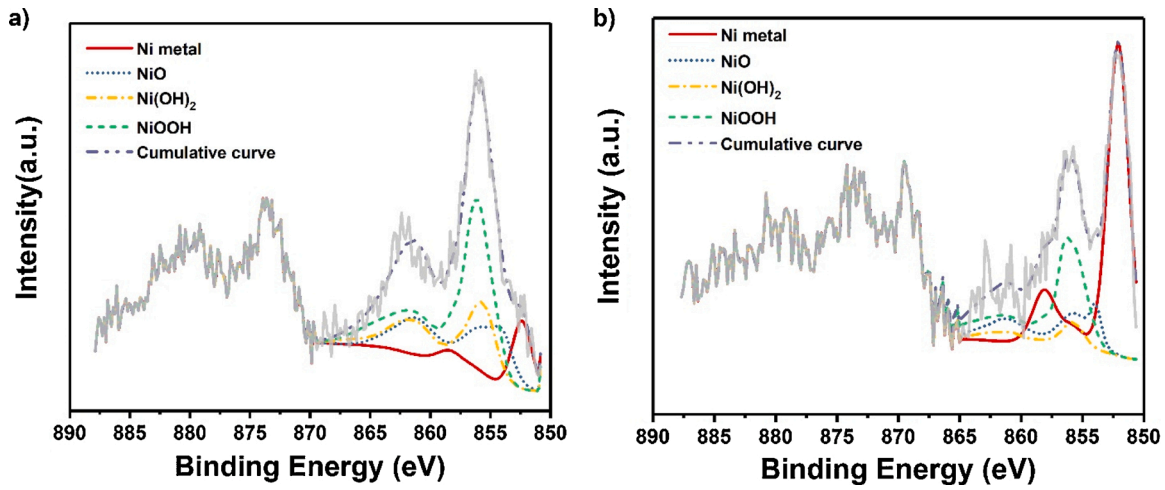

Fig. 7. Ni 2p spectra of a) Ni/Al_2O_3 and b) $1Ni\text{-}2Ga/Al_2O_3$.

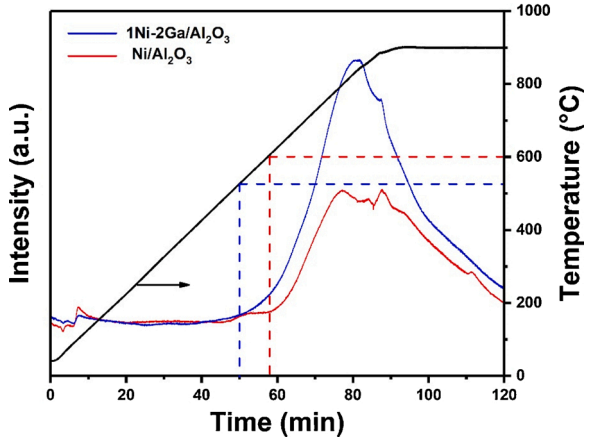

Fig. 8. H_2-TPR profiles for Ni/Al_2O_3 and $1Ni\text{-}2Ga/Al_2O_3$.The dashed lines mark the approximate onset of the reduction peak.

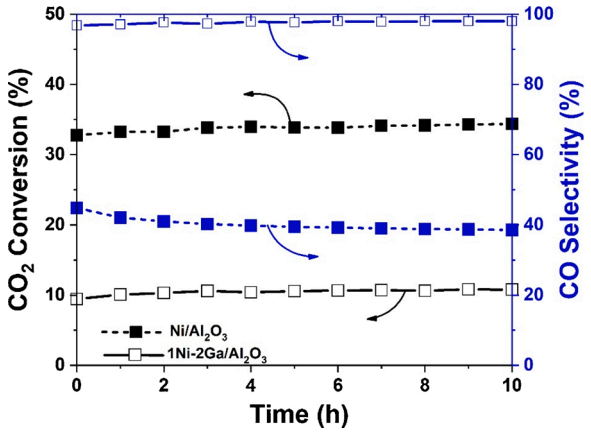

Fig. 9. CO_2 conversion and CO selectivity for Ni/Al_2O_3 and $1Ni\text{-}2Ga/Al_2O_3$ at 400 °C upon in-situ catalyst reduction at 830 °C for 1 h prior to the test.

comparison. No diffraction peak for Ni or NiO was observed for both the fresh and spent catalysts (Fig. S11). For $1Ni\text{-}2Ga/Al_2O_3$, no sign of Ga was observed in the diffraction patterns. This suggests that no large crystalline nanoparticles (> 3 nm) of Ni, NiO or Ga_2O_3 were formed in the fresh or spent catalysts either during the calcination, reduction, or reaction. To confirm these observations, we also took STEM images of the $1Ni\text{-}2Ga/Al_2O_3$ after 20 h of reaction (Fig. S12). No sign of Ni and/or Ga agglomeration and sintering could be detected, confirming that $1Ni\text{-}2Ga/Al_2O_3$ did not sinter during the reaction.

4. Conclusions

Ni-based catalysts are known for their tendency to form CH_4 during the CO_2 hydrogenation reaction. Although they are usually more thermally robust compared to Cu-based catalysts, they are not used for the RWGS due to their low selectivity for CO. This was also confirmed by our experiments using a Ni/Al_2O_3 catalyst. However, our present study showed that addition of Ga can restructure Ni particles on the surface of alumina in a way, which increased the selectivity for CO. Although this shift in selectivity came at the expense of lower catalyst activity, selective formation of CO eliminates the need for downstream separation processing in industrial applications. The lower CO_2 conversion could be compensated by recycling the unreacted gases to increase the overall conversion. Using in-situ DRIFTS studies as well as other catalyst characterization methods showed that the addition of Ga led to high dispersion of Ni and high surface coverage of alumina, which limited the availability of hydroxyl groups on the surface. Our results support the view that hydroxyl groups are crucial species in the CO_2 hydrogenation mechanism since they are the active sites for CO_2 adsorption and formation of bicarbonates and their presence contributed to the higher activity of Ni/Al_2O_3 compared to $1Ni\text{-}2Ga/Al_2O_3$. Although Ga is more expensive compared to Ni and the addition of Ga does not seem economically promising, this disadvantage is compensated by the better temperature stability of these catalysts, which might help the process in the long run. Nevertheless, further studies will be required to increase their activity.

CRediT authorship contribution statement

Ali M. Bahmanpour: Conceptualization, Methodology, Formal analysis, Investigation, Validation, Writing – original draft, Data curation. **Rob Jeremiah G. Nuguid:** Investigation, Data curation, Writing – original draft. **Louisa M. Savereide:** Investigation, Data curation, Validation, Writing – original draft. **Mounir D. Mensi:** Investigation, Data curation, Writing – original draft. **Davide Ferri:** Supervision, Resources, Writing – review & editing. **Jeremy S. Luterbacher:** Supervision, Resources, Writing – review & editing. **Oliver Kröcher:** Supervision, Resources, Project administration, Writing – review & editing.

Declaration of Competing Interest

The authors declare that they have no known competing financial interests or personal relationships that could have appeared to influence the work reported in this paper.

Acknowledgments

JSL, and LMS acknowledge funding from the European Research Council (ERC) under the European Union's Horizon 2020 research and innovation program (Starting grant: CATACOAT, No. 758653). RJGN, DF, and O.K. acknowledge funding from the Swiss National Science Foundation (SNF, #172669). The authors would like to acknowledge Dr. Pascal Schouwink for XRD analysis, and Mr Sylvain Coudret for ICP-OES analysis.

Appendix A. Supplementary data

Supplementary material related to this article can be found, in the online version, at doi:https://doi.org/10.1016/j.jcou.2021.101881.

References

[1] J.C. Zachos, G.R. Dickens, R.E. Zeebe, An early Cenozoic perspective on greenhouse warming and carbon-cycle dynamics, Nature 451 (2008) 279–283, https://doi.org/10.1038/nature06588.
[2] W. Wang, S. Wang, X. Ma, J. Gong, Recent advances in catalytic hydrogenation of carbon dioxide, Chem. Soc. Rev. 40 (2011) 3703–3727, https://doi.org/10.1039/C1CS15008A.
[3] Y. Lou, F. jiang, W. Zhu, L. Wang, T. Yao, S. Wang, B. Yang, B. Yang, Y. Zhu, X. Liu, CeO2 supported Pd dimers boosting CO2 hydrogenation to ethanol, Appl. Catal. B Environ. 291 (2021), https://doi.org/10.1016/j.apcatb.2021.120122.
[4] Q. Wang, S. Santos, C.A. Urbina-Blanco, W.Y. Hernández, M. Impéror-Clerc, E. I. Vovk, M. Marinova, O. Ersen, W. Baaziz, O.V. Safonova, A.Y. Khodakov, M. Saeys, V.V. Ordomsky, Solid micellar Ru single-atom catalysts for the water-free hydrogenation of CO2 to formic acid, Appl. Catal. B Environ. 290 (2021), https://doi.org/10.1016/j.apcatb.2021.120036.
[5] J. Graciani, K. Mudiyanselage, F. Xu, A.E. Baber, J. Evans, S.D. Senanayake, D. J. Stacchiola, P. Liu, J. Hrbek, J. Fernández Sanz, J.A. Rodriguez, Highly active copper-ceria and copper-ceria-titania catalysts for methanol synthesis from CO2, Science 345 (2014) 546–550, https://doi.org/10.1126/science.1253057.
[6] P. Gao, S. Li, X. Bu, S. Dang, Z. Liu, H. Wang, L. Zhong, M. Qiu, C. Yang, J. Cai, W. Wei, Y. Sun, Direct conversion of CO2 into liquid fuels with high selectivity over a bifunctional catalyst, Nat. Chem. 9 (2017) 1019–1024, https://doi.org/10.1038/nchem.2794.
[7] J. Wei, Q. Ge, R. Yao, Z. Wen, C. Fang, L. Guo, H. Xu, J. Sun, Directly converting CO2 into a gasoline fuel, Nat. Commun. 8 (2017), https://doi.org/10.1038/ncomms15174.
[8] M.D. Porosoff, B. Yan, J.G. Chen, Catalytic reduction of CO2 by H2 for synthesis of CO, methanol and hydrocarbons: challenges and opportunities, Energy Environ. Sci. 9 (2016) 62–73, https://doi.org/10.1039/c5ee02657a.
[9] X. Zhang, X. Zhu, L. Lin, S. Yao, M. Zhang, X. Liu, X. Wang, Y.-W. Li, C. Shi, D. Ma, Highly dispersed copper over β-Mo2C as an efficient and stable catalyst for the reverse water gas shift (RWGS) reaction, ACS Catal. 7 (2017) 912–918, https://doi.org/10.1021/acscatal.6b02991.
[10] X. Yang, X. Su, X. Chen, H. Duan, B. Liang, Q. Liu, X. Liu, Y. Ren, Y. Huang, T. Zhang, Promotion effects of potassium on the activity and selectivity of Pt/zeolite catalysts for reverse water gas shift reaction, Appl. Catal. B Environ. 216 (2017) 95–105, https://doi.org/10.1016/j.apcatb.2017.05.067.
[11] D.H. Kim, J.L. Park, E.J. Park, Y.D. Kim, S. Uhm, Dopant effect of barium zirconate-based perovskite-type catalysts for the intermediate-temperature reverse water gas shift reaction, ACS Catal. 4 (2014) 3117–3122, https://doi.org/10.1021/cs500476e.
[12] L. Pastor-Pérez, F. Baibars, E. Le Sache, H. Arellano-García, S. Gu, T.R. Reina, CO2 valorisation via Reverse Water-Gas Shift reaction using advanced Cs doped Fe-Cu/Al2O3 catalysts, J. CO2 Util. 21 (2017) 423–428, https://doi.org/10.1016/j.jcou.2017.08.009.
[13] Q. Zhang, L. Pastor-Pérez, W. Jin, S. Gu, T.R. Reina, Understanding the promoter effect of Cu and Cs over highly effective B-Mo2C catalysts for the reverse water-gas shift reaction, Appl. Catal. B Environ. 244 (2019) 889–898, https://doi.org/10.1016/j.apcatb.2018.12.023.
[14] B. Yao, T. Xiao, O.A. Makgae, X. Jie, S. Gonzalez-Cortes, S. Guan, A.I. Kirkland, J. R. Dilworth, H.A. Al-Megren, S.M. Alshihri, P.J. Dobson, G.P. Owen, J.M. Thomas, P.P. Edwards, Transforming carbon dioxide into jet fuel using an organic combustion-synthesized Fe-Mn-K catalyst, Nat. Commun. 11 (2020), https://doi.org/10.1038/s41467-020-20214-z.
[15] S. Kattel, W. Yu, X. Yang, B. Yan, Y. Huang, W. Wan, P. Liu, J.G. Chen, CO2 hydrogenation over oxide-supported PtCo catalysts: the role of the oxide support in determining the product selectivity, Angew. Chem. - Int. Ed. 55 (2016) 7968–7973, https://doi.org/10.1002/anie.201601661.
[16] S. Kattel, B. Yan, Y. Yang, J.G. Chen, P. Liu, Optimizing binding energies of key intermediates for CO2 hydrogenation to methanol over oxide-supported copper, J. Am. Chem. Soc. 138 (2016) 12440–12450, https://doi.org/10.1021/jacs.6b05791.
[17] S. Kattel, P. Liu, J.G. Chen, Tuning selectivity of CO2 hydrogenation reactions at the metal/oxide interface, J. Am. Chem. Soc. 139 (2017) 9739–9754, https://doi.org/10.1021/jacs.7b05362.
[18] S. Kattel, B. Yan, J.G. Chen, P. Liu, CO2 hydrogenation on Pt, Pt/SiO2 and Pt/TiO2: importance of synergy between Pt and oxide support, J. Catal. 343 (2016) 115–126, https://doi.org/10.1016/j.jcat.2015.12.019.
[19] S. Kattel, P.J. Ramírez, J.G. Chen, J.A. Rodriguez, P. Liu, Active sites for CO2 hydrogenation to methanol on Cu/ZnO catalysts, Science 355 (2017) 1296–1299, https://doi.org/10.1126/science.aal3573.
[20] A.M. Bahmanpour, M. Signorile, O. Kröcher, Recent progress in syngas production via catalytic CO2 hydrogenation reaction, Appl. Catal. B Environ. 295 (2021), 120319, https://doi.org/10.1016/j.apcatb.2021.120319.
[21] Y. Ma, Z. Guo, Q. Jiang, K.-H. Wu, H. Gong, Y. Liu, Molybdenum carbide clusters for thermal conversion of CO2 to CO via reverse water-gas shift reaction, J. Energy Chem. 50 (2020) 37–43, https://doi.org/10.1016/j.jechem.2020.03.012.
[22] M.D. Porosoff, X. Yang, J.A. Boscoboinik, J.G. Chen, Molybdenum carbide as alternative catalysts to precious metals for highly selective reduction of CO2 to CO, Angew. Chem. - Int. Ed. 53 (2014) 6705–6709, https://doi.org/10.1002/anie.201404109.
[23] A.M. Bahmanpour, F. Héroguel, M. Kılıç, C.J. Baranowski, L. Artiglia, U. Röthlisberger, J.S. Luterbacher, O. Kröcher, Cu–Al spinel as a highly active and stable catalyst for the reverse water gas shift reaction, ACS Catal. 9 (2019) 6243–6251, https://doi.org/10.1021/acscatal.9b01822.
[24] A.M. Bahmanpour, F. Héroguel, M. Kılıç, C.J. Baranowski, P. Schouwink, U. Röthlisberger, J.S. Luterbacher, O. Kröcher, Essential role of oxygen vacancies of Cu-Al and Co-Al spinel oxides in their catalytic activity for the reverse water gas shift reaction, Appl. Catal. B Environ. 266 (2020), 118669, https://doi.org/10.1016/j.apcatb.2020.118669.
[25] A.M. Bahmanpour, B.P. Le Monnier, Y.-P. Du, F. Héroguel, J.S. Luterbacher, O. Kröcher, Increasing the activity of the Cu/CuAl2O4/Al2O3 catalyst for the RWGS through preserving the Cu2+ ions, Chem. Commun. 57 (2021) 1153–1156, https://doi.org/10.1039/D0CC07142K.
[26] M.S. Duyar, C. Tsai, J.L. Snider, J.A. Singh, A. Gallo, J.S. Yoo, A.J. Medford, F. Abild-Pedersen, F. Studt, J. Kibsgaard, S.F. Bent, J.K. Nørskov, T.F. Jaramillo, A highly active molybdenum phosphide catalyst for methanol synthesis from CO and CO2, Angew. Chem. Int. Ed. 57 (2018) 15045–15050, https://doi.org/10.1002/anie.201806583.
[27] L. Lin, J. Liu, X. Liu, Z. Gao, N. Rui, S. Yao, F. Zhang, M. Wang, C. Liu, L. Han, F. Yang, S. Zhang, X. Wen, S.D. Senanayake, Y. Wu, X. Li, J.A. Rodriguez, D. Ma, Reversing sintering effect of Ni particles on γ-Mo2N via strong metal support interaction, Nat. Commun. 12 (2021) 6978, https://doi.org/10.1038/s41467-021-27116-8.
[28] S. Li, J. Yang, C. Song, Q. Zhu, D. Xiao, D. Ma, Iron Carbides, Control synthesis and catalytic applications in COx hydrogenation and electrochemical HER, Adv. Mater. 31 (2019), 1901796, https://doi.org/10.1002/adma.201901796.
[29] A. Aitbekova, L. Wu, C.J. Wrasman, A. Boubnov, A.S. Hoffman, E.D. Goodman, S. R. Bare, M. Cargnello, Low-temperature restructuring of CeO2-supported Ru nanoparticles determines selectivity in CO2 catalytic reduction, J. Am. Chem. Soc. 140 (2018) 13736–13745, https://doi.org/10.1021/jacs.8b07615.
[30] J.H. Kwak, L. Kovarik, J. Szanyi, Heterogeneous catalysis on atomically dispersed supported metals: CO 2 reduction on multifunctional Pd catalysts, ACS Catal. 3 (2013) 2094–2100, https://doi.org/10.1021/cs4001392.
[31] J.C. Matsubu, V.N. Yang, P. Christopher, Isolated metal active site concentration and stability control catalytic CO2 reduction selectivity, J. Am. Chem. Soc. 137 (2015) 3076–3084, https://doi.org/10.1021/ja5128133.
[32] S. Li, Y. Xu, Y. Chen, W. Li, L. Lin, M. Li, Y. Deng, X. Wang, B. Ge, C. Yang, S. Yao, J. Xie, Y. Li, X. Liu, D. Ma, Tuning the selectivity of catalytic carbon dioxide hydrogenation over iridium/cerium oxide catalysts with a strong metal–support interaction, Angew. Chem. Int. Ed. 56 (2017) 10761–10765, https://doi.org/10.1002/anie.201705002.
[33] J. Ye, Q. Ge, C.-J. Liu, Effect of PdIn bimetallic particle formation on CO2 reduction over the Pd-In/SiO2 catalyst, Chem. Eng. Sci. 135 (2015) 193–201, https://doi.org/10.1016/j.ces.2015.04.034.
[34] B. Liang, H. Duan, X. Su, X. Chen, Y. Huang, X. Chen, J.J. Delgado, T. Zhang, Promoting role of potassium in the reverse water gas shift reaction on Pt/mullite catalyst, Catal. Today 281 (2017) 319–326, https://doi.org/10.1016/j.cattod.2016.02.051.
[35] H. Xu, X. Luo, J. Wang, Y. Su, X. Zhao, Y. Li, Spherical sandwich Au@Pd@UIO-67/Pt@UIO- n (n = 66, 67, 69) core-shell catalysts: Zr-based metal-organic frameworks for effectively regulating the reverse water-gas shift reaction, ACS Appl. Mater. Interfaces 11 (2019) 20291–20297, https://doi.org/10.1021/acsami.9b04748.
[36] Y. Han, H. Xu, Y. Su, Z.-L. Xu, K. Wang, W. Wang, Noble metal (Pt, Au@Pd) nanoparticles supported on metal organic framework (MOF-74) nanoshuttles as high-selectivity CO2 conversion catalysts, J. Catal. 370 (2019) 70–78, https://doi.org/10.1016/j.jcat.2018.12.005.
[37] B. Yan, B. Zhao, S. Kattel, Q. Wu, S. Yao, D. Su, J.G. Chen, Tuning CO2 hydrogenation selectivity via metal-oxide interfacial sites, J. Catal. 374 (2019) 60–71, https://doi.org/10.1016/j.jcat.2019.04.036.

[38] A. Ranjbar, A. Irankhah, S.F. Aghamiri, Catalytic activity of rare earth and alkali metal promoted (Ce, La, Mg, K) Ni/Al2O3 nanocatalysts in reverse water gas shift reaction, Res. Chem. Intermed. 45 (2019) 5125–5141, https://doi.org/10.1007/s11164-019-03905-1.

[39] N. Nityashree, C.A.H. Price, L. Pastor-Perez, G.V. Manohara, S. Garcia, M. M. Maroto-Valer, T.R. Reina, Carbon stabilised saponite supported transition metal-alloy catalysts for chemical CO2 utilisation via reverse water-gas shift reaction, Appl. Catal. B Environ. 261 (2020), https://doi.org/10.1016/j.apcatb.2019.118241.

[40] C.A.H. Price, L. Pastor-Perez, T.R. Reina, J. Liu, Yolk-Shell structured NiCo@SiO2 nanoreactor for CO2 upgrading via reverse water-gas shift reaction, Catal. Today 383 (2020) 358–367, https://doi.org/10.1016/j.cattod.2020.09.018, 1 January 2022.

[41] C. Tsounis, Y. Wang, H. Arandiyan, R.J. Wong, C.Y. Toe, R. Amal, J. Scott, Tuning the Selectivity of LaNiO3 Perovskites for CO2 hydrogenation through potassium substitution, Catalysts 10 (2020), https://doi.org/10.3390/catal10040409.

[42] H. Zhang, H. Xu, Y. Li, Y. Su, Octahedral core–shell bimetallic catalysts M@UIO-67 (M = Pt–Pd nanoparticles, Pt–Pd nanocages): metallic nanocages that enhanced CO2 conversion, Appl. Mater. Today 19 (2020), 100609, https://doi.org/10.1016/j.apmt.2020.100609.

[43] J.R. Morse, M. Juneau, J.W. Baldwin, M.D. Porosoff, H.D. Willauer, Alkali promoted tungsten carbide as a selective catalyst for the reverse water gas shift reaction, J. CO2 Util. 35 (2020) 38–46, https://doi.org/10.1016/j.jcou.2019.08.024.

[44] O. Arbeláez, T.R. Reina, S. Ivanova, F. Bustamante, A.L. Villa, M.A. Centeno, J. A. Odriozola, Mono and bimetallic Cu-Ni structured catalysts for the water gas shift reaction, Appl. Catal. Gen. 497 (2015) 1–9, https://doi.org/10.1016/j.apcata.2015.02.041.

[45] J. Li, X. Mei, L. Zhang, Z. Yu, Q. Liu, T. Wei, W. Wu, D. Dong, L. Xu, X. Hu, A comparative study of catalytic behaviors of Mn, Fe, Co, Ni, Cu and Zn–based catalysts in steam reforming of methanol, acetic acid and acetone, Int. J. Hydrogen Energy 45 (2020) 3815–3832, https://doi.org/10.1016/j.ijhydene.2019.03.269.

[46] E. Le Saché, L. Pastor-Pérez, B.J. Haycock, J.J. Villora-Picó, A. Sepúlveda-Escribano, T.R. Reina, Switchable catalysts for chemical CO2 recycling: a step forward in the methanation and reverse water-gas shift reactions, ACS Sustain. Chem. Eng. 8 (2020) 4614–4622, https://doi.org/10.1021/acssuschemeng.0c00551.

[47] A.H. Braga, N.J.S. Costa, K. Philippot, R.V. Gonçalves, J. Szanyi, L.M. Rossi, Structure and activity of supported bimetallic NiPd nanoparticles: influence of preparation method on CO2 reduction, ChemCatChem 12 (11) (2020) 2967–2976, https://doi.org/10.1002/cctc.201902329. June 2020.

[48] R.C. Cammarota, M.V. Vollmer, J. Xie, J. Ye, J.C. Linehan, S.A. Burgess, A. M. Appel, L. Gagliardi, C.C. Lu, A bimetallic nickel-gallium complex catalyzes CO2 hydrogenation via the intermediacy of an anionic d10 nickel hydride, J. Am. Chem. Soc. 139 (2017) 14244–14250, https://doi.org/10.1021/jacs.7b07911.

[49] F. Studt, I. Sharafutdinov, F. Abild-Pedersen, C.F. Elkjær, J.S. Hummelshøj, S. Dahl, I. Chorkendorff, J.K. Nørskov, Discovery of a Ni-Ga catalyst for carbon dioxide reduction to methanol, Nat. Chem. 6 (2014) 320–324, https://doi.org/10.1038/nchem.1873.

[50] H. Harms, B. Höhlein, A. Skov, Methanisierung kohlenmonoxidreicher Gase beim Energie-Transport, Chem. Ing. Tech. 52 (1980) 504–515, https://doi.org/10.1002/cite.330520605.

[51] R.J.G. Nuguid, D. Ferri, O. Kröcher, Design of a reactor cell for modulated excitation Raman and diffuse reflectance studies of selective catalytic reduction catalysts, Emiss. Control Sci. Technol. 5 (2019) 307–316, https://doi.org/10.1007/s40825-019-00141-2.

[52] L.F. Bobadilla, J.L. Santos, S. Ivanova, J.A. Odriozola, A. Urakawa, Unravelling the role of oxygen vacancies in the mechanism of the reverse water-gas shift reaction by Operando DRIFTS and ultraviolet-visible spectroscopy, ACS Catal. 8 (2018) 7455–7467, https://doi.org/10.1021/acscatal.8b02121.

[53] X. Wang, H. Shi, J. Szanyi, Controlling selectivities in CO2 reduction through mechanistic understanding, Nat. Commun. 8 (2017), https://doi.org/10.1038/s41467-017-00558-9.

[54] X. Wang, H. Shi, J.H. Kwak, J. Szanyi, Mechanism of CO2 hydrogenation on Pd/Al2O3 catalysts: kinetics and transient DRIFTS-MS studies, ACS Catal. 5 (2015) 6337–6349, https://doi.org/10.1021/acscatal.5b01464.

[55] C.-S. Chen, W.-H. Cheng, S.-S. Lin, Mechanism of CO formation in reverse water-gas shift reaction over Cu/Al2O3 catalyst, Catal. Lett. 68 (2000) 45–48.

[56] L.R. Winter, E. Gomez, B. Yan, S. Yao, J.G. Chen, Tuning Ni-catalyzed CO2 hydrogenation selectivity via Ni-ceria support interactions and Ni-Fe bimetallic formation, Appl. Catal. B Environ. 224 (2018) 442–450, https://doi.org/10.1016/j.apcatb.2017.10.036.

[57] M.M. Schubert, H.A. Gasteiger, R.J. Behm, Surface formates as side products in the selective CO oxidation on Pt/γ-Al2O3, J. Catal. 172 (1997) 256–258, https://doi.org/10.1006/jcat.1997.1856.

[58] C. Yang, R. Mu, G. Wang, J. Song, H. Tian, Z.-J. Zhao, J. Gong, Hydroxyl-mediated ethanol selectivity of CO2 hydrogenation, Chem. Sci. 10 (2019) 3161–3167, https://doi.org/10.1039/C8SC05608K.

[59] M.C. Biesinger, B.P. Payne, A.P. Grosvenor, L.W.M. Lau, A.R. Gerson, R.S.C. Smart, Resolving surface chemical states in XPS analysis of first row transition metals, oxides and hydroxides: Cr, Mn, Fe, Co and Ni, Appl. Surf. Sci. 257 (2011) 2717–2730, https://doi.org/10.1016/j.apsusc.2010.10.051.